The Implementation of QM/MM on Non-Adiabatic Dynamics Using AMBER and NEXMD

Dustin Tracy

January 27, 2021

Contents

Masterfile

```
\documentclass[editMode]{ufdissertation}\sloppy
\usepackage{tikz}%        tikz is used by almost everyone, but certainly by me for thi
\usepackage{bm}%          bm is needed in order to boldface mathematical symbols
%% Uncomment the relevant line below if you have tables or figures.
\haveTablestrue%          Uncomment this if you have tables in your thesis.
\haveFigurestrue%         Uncomment this if you have figures in your thesis.
\haveObjectstrue%         Uncomment this if you have Objects in your thesis. This is al

\title{The Implementation of QM/MM on Non-Adiabatic Dynamics Using AMBER and NEXMD}%

\degreeType{Doctorate of Philosophy}%   Official name of your degree; eg "Doctorate o
\major{Mathematics}%                    Your official Department
\author{Dustin Tracy}%                  Your Name
\thesisType{Dissertation}%              Dissertation (PhD) or Thesis (Masters)
\degreeYear{2021}%                      Intended graduation year (not the year you su
\degreeMonth{May}%                      Month of graduation should be May, August, or De
\chair{Adrian Roitberg}%                Chair and Cochair (see comment block above

%%%%%%%%%%%%%%%%%%%%%%%%%%%%%%%%%%%%%%%%%%%%%%%%%%%%%%%%%%%%%%%%%%%%%%%%%%%%%%%%%%%%%%%%%
%%% For each of the following, type in the name of the file that contains each section
%        They are assumed to be tex files, but if they aren't the command takes an optio
```

```latex
%           So, you could load dedication.tex as your dedication file using \setDedication
%           You could load dedication.txt instead with \setDedicationFile[txt]{dedication}
%           NOTE: For some compilers they may or may not add a .tex to the end of the file
%               If you get a "couldn't find dedication.tex.tex" type error, try the comman
%               e.g. \setDedicationFile[]{dedication}
%%%
%%%%%%%%%%%%%%%%%%%%%%%%%%%%%%%%%%%%%%%%%%%%%%%%%%%%%%%%%%%%%%%%%%%%%%%%%%%%%%%%%%%%

%%% These are REQUIRED sections; easiest to do via these commands.

\setDedicationFile{dedicationFile}%                  Dedication Page
\setAcknowledgementsFile{acknowledgementsFile}%      Acknowledgements Page
\setAbstractFile{abstractFile}%                      Abstract Page (This should only in
\setReferenceFile{thesis.bib}{amsplain}%        References. First argument is your bi
%                                                   the second argument is your bi
\setBiographicalFile{biographyFile}%                 Biography file of the Author (you)

%%% These are NOT required, so only use them if you actually need/have them.

% \setAbbreviationsFile{abbreviations}%              Abbreviations Page
% \setAppendixFile{appendix}%                        Appendix Content; hyperlinking might
% \multipleAppendixtrue%                             Uncomment this if you have more than
%                                                   comment it if you have only one ap


%%%%%%                          End of File Assignment
%%%%%%%%%%%%%%%%%%%%%%%%%%%%%%%%%%%%%%%%%%%%%%%%%%%%%%%%%%%%%%%%%%%%%%%%%%%%%%%%%%

\begin{document}
%%% Here you just need to include/input your actual work.
%           The above files (dedication, acknowledgement, titlepage, etc etc) will all be
%           using the files you assigned above.
%           If you want to input the above files manually you can comment out the \setFILE
%           and use \input or \include here. Generally you want to use \include to get you
%           NOTE: If you input manually you will have to do some/all the formatting manual



% \include{chapter1}% Modified from old template.
\include{theoreticalMethods}% Modified from old template.
```

```
% \include{chapter3}% Modified from old template.
% \include{chapter4}% Modified from old template.
% \include{chapter5}% Modified from old template.

% \begin{algorithm}% Example showing the weird "algorithm" environment works...
%       \captionof{algorithm}{Test Caption}
% \end{algorithm}
% \addObject{TestStuff!}%      This is probably the command that a normal author will us

\chapter{EXAMPLES OF EDITOR/Author TOOLS, TABLES, AND IMAGES}% Notice that we can use c
\input{editorAndAuthorRemarks}%      Stuff about using editorRemark and authorRemark com
% \input{includingTablesExamples}%    Stuff about using Tables.
% \input{includingImagesExamples}%    Stuff about using Images.

\end{document}
```

Dedication

I dedicate this work to my loving wife Sarah Stern, who's love I will alway cherish.
I also dedicate this work to my Grandmother Jean Tracy, who encouraged me to work for r

Acknowledgements

I'd like to thank all the amazing individuals who have supported me in this effort.
I'd like to give special thanks to my advisor Adrian Roitberg, who's patience, guidance

Biographical Sketch

Though many people call me Dustin; actually.... I'm Batman!

Abstract

We present a method to link the Non-adiabatic-Excited-state Molecular Dynamics (NEXMD)
NEXMD is a computational package particularly developped to perform simulations of the
In this work, we use it solely for its capability to perform excited-state adiabatic dy
In this report, we first describe the basic methodology behind the code, where we brief
We outline the flowchart connecting them in order to optimize their exchange allowing e

To validate functionality, we analyze the dynamics of a polyphenylene vinylene oligomer
We highlight the system's ability to generate optical spectrum, view state-dependent co

Introduction

Theoretial Methods

\chapter{Theoretical Methods} \label{theoreticalMethods}

\section{Secular Determinants}

The goal of computational chemistry is to solve the Schrodinger equation.
Solving it completely is only possible for very small subsets of possible situations.
In most cases, significant approximations must be made.
One of the more common such approximations, is the appoximation of the atomic basis fun
If we write the Schodinger equation as

\begin{equation} \label{eq:oneeenergy}
E(\Psi) = \frac{\left<\right.\Psi\left|\right.\bm{H}\left.\right|\Psi\left>\right.}{\le
\end{equation}

where $\mathbf{H}$ the Hamiltonian, E is the energy of the
system, and Ψ is a wavefunction that describes the system.
Ψ will be some linear combination of functions $\Psi=\sum_{i}c_i\psi_i$.
We can now expand the numerator and denominator of the right-hand side of equation \re

\begin{align}
  \label{eq:variation1}
  \left<\right.\Psi\left|\right.\bm{H}\left.\right|\Psi\left>\right.&=
      \left(\sum_{i} c_i \psi_i \right) \mathbf{H} \left(\sum_j c_j \psi_j \right) &
        \left<\right.\Psi\left.\right|\left.\Psi\left.\right.\right>&=
      \left(\sum_{i} c_i \psi_i \right) \left(\sum_j c_j \psi_j \right) \\
    &= \sum_{ij} c_{i}c_j H_{ij} & &= \sum_{ij} c_{i}c_j S_{ij}
  \label{eq:variation2}
\end{align}

Taking the partial derivatives of both sides with respect to a_i in
equation \ref{eq:variation2} provides us with

```latex
\begin{align}
  \label{eq:variationexpansion}
  \frac{\partial}{\partial c_{\alpha}}
  \left<\right.\Psi\left|\right.\bm{H}\left.\right|\Psi\left>\right.&=
      2c_\alpha H_{\alpha \alpha} + \sum_{\alpha j \neq \alpha} 2c_j H_{\alpha j} &
    \frac{\partial}{\partial c_{\alpha}}
    \left<\right.\Psi\left.\right|\left.\Psi\left.\right.\right>&=
  2 c_\alpha S_{\alpha\alpha} + \sum_{\alpha j \neq \alpha} c_j S_{\alpha j}
\end{align}

If we multiply both sides of equation \ref{eq:oneeenergy} by
$\left<\right.\Psi\left.\right|\left.\Psi\left.\right.\right>$ and
take the partial derivative with respect to $c_{\alpha}$,

\begin{align}
  \frac{\partial}{\partial c_{\alpha}}
  \left( E \left<\right.\Psi\left.\right|\left.\Psi\left.\right.\right> \right)&=
 \frac{\partial}{\partial c_{\alpha}}
 \left<\right.\Psi\left|\right.\bm{H}\left.\right|\Psi\left>\right. \\
  \label{eq:variation3}
  E \frac{\partial \left<\right.\Psi\left.\right|\left.\Psi\left.\right.\right>}{\part:
  + \left<\right.\Psi\left.\right|\left.\Psi\left.\right.\right> \frac{\partial E}{\par
  \frac{\partial}{\partial c_{\alpha}}
  \left<\right.\Psi\left|\right.\bm{H}\left.\right|\Psi\left>\right.
\end{align}

Now we minimize $E$ by rearranging equation \ref{eq:variation3}

\begin{equation}
  \frac{\partial E}{\partial c_{\alpha}} =
  \frac{1}{\left<\right.\Psi\left.\right|\left.\Psi\left.\right.\right>}
  \left[
    \frac{\left<\right.\Psi\left|\right.\bm{H}\left.\right|\Psi\left>\right.}
    {\partial c_{\alpha}}
    -E \frac{\left<\right.\Psi\left.\right|\left.\Psi\left.\right.\right>}
    {\partial c_{\alpha}}
  \right] = 0
\end{equation}

Substituting our results from equation \ref{eq:variationexpansion} and
```

dividing by common multipliers, we find

```
\begin{equation}
  c_{\alpha} H_{\alpha \alpha} + \sum_{\alpha j \neq \alpha} c_j H_{\alpha j} -
  E \left( c_{\alpha} S_{\alpha \alpha} + \sum_{\alpha j \neq \alpha} c_j S_{\alpha j}
\end{equation}

\begin{equation}
  c_{\alpha} H_{\alpha \alpha} + \sum_{\alpha j \neq \alpha} c_j H_{\alpha j} -
  E \left( c_{\alpha} S_{\alpha \alpha} + \sum_{\alpha j \neq \alpha} c_j S_{\alpha j}
\end{equation}
```

which is often referred to as the matrix form of the Schrodinger
equation. A more intuitive understanding of the equation may be had
if we expand out for $\alpha=1-3$.

```
\begin{equation} \label{eq:SchrodingerMatrix}
  \begin{bmatrix}
    H_{11}-ES_{11} & H_{12}-ES_{12} & H_{13}-ES_{13} \\
    H_{21}-ES_{21} & H_{22}-ES_{22} & H_{23}-ES_{23} \\
    H_{31}-ES_{31} & H_{32}-ES_{32} & H_{33}-ES_{33}
  \end{bmatrix}
  \begin{bmatrix}
    c_1 \\
    c_2 \\
    c_3
  \end{bmatrix} = 0
\end{equation}
```

This equation can be rewritten simply as $Hc=ESc$. The determinant
$\left| H-ES \right|$ is known as the secular determinant, with
eigenvalues corresponding to the energies of the molecular orbitals,
whose characteristics are determined by the coefficients in the
corresponding eigenvector.\textbf{cite:Engel2006}

\section{Hartree Fock}
    Before we can solve the secular equation we need to know our
    Hamiltonian. We begin with the generalized Hamiltonian of a
    molecular system,\cite{Engel2006}

```
\begin{align} \label{eq:fullhamiltonian}
  \begin{split}
  \bm{H} =& -\frac{\hbar^2}{2m_e}\sum_i^{electrons}\nabla_i^2-\frac{\hbar^2}{2}\sum
  & + \frac{e^2}{4\pi\varepsilon_0}\sum_{i}^{electrons}\sum_{j<i}^{electrons}\frac
  \end{split}
\end{align}
```

where n is summed over all the nuclei, and the i and j are summed over the el
With this Hamiltonian, the secular equation is near impossible to solve without son
The one most relevant to our work is the adiabatic approximation, also known as the
The potential energy surface then, can be extrapolated by applying the electronic H
In the mean field approximation, each electron feels the average potential of all t
The electronic parts the Hamiltonian are now decoupled, and the total Hamiltonian of
In actuality the electrons of one orbit will effect electrons of the orbit of anotl
The electrons will want to avoid each-other and their paths will change accordingl
This approximation to the method fails to take this into account.
We call the difference between the actual energy E and the Hartree-Fock energy $'
coulomb correlation energy $E_{corrrelation}$.
%There have been numerous ways developed to help alleviate this problem, including

The total many electron wavefunction must satisfy the Pauli-Exclusion principle.
We can fulfill that requirement, if we assume that it is a single slater-determinar

```
\begin{equation} \label{eq:slater-determinant} \phi(\bm{r};\bm{R}) =
  \left|p \cdots s\right> = \frac{1}{\sqrt{N}}
  \begin{vmatrix}
\chi_{p}(\bm{r}_1) & \cdots & \cdots \chi_{s}(\bm{r}_1) \\
\vdots            & \ddots          &      \vdots       \\
\chi_{p}(\bm{r}_n) & \cdots & \cdots \chi_{s}(\bm{r}_n)
  \end{vmatrix}
\end{equation}
```

where ϕ is the electron coordinates that depend parametrically on the
nuclear coordinates. The $p \cdots s$ are the subscripts of the
molecular orbitals, and $1 \cdots n$ are the indices for the
electrons.

Finally, things simplify greatly if the molecular orbitals are
othornormal to each other. $\left<\right.i\left|\right.j\left>\right. = \delta_{ij}$
Intuition tells us that because the Hamiltonian is an operator that

acts on at most 2 electrons at a time, and the electron orbitals
are orthonormal, any perturbation beyond 2 will integrate to 0. In
fact, there's a whole set of rules to reduce electron integral
summations called the Slater-Condon rules.\textbf{CITE}

\begin{enumerate}
\item
  $ \left | \cdots mn \cdots \right > \rightarrow \left | \cdots mn
\cdots \right > \Rightarrow \sum_i \left< i \right| h \left| i
  \right> + \frac{1}{2} \sum_{ij} \left< ij \right|\left| ij \right> $
\item
  $ \left | \cdots mn \cdots \right > \rightarrow \left | \cdots pn
\cdots \right > \Rightarrow \left< i \right| h \left| i \right> +
  \sum_{i} \left<mi \right|\left| pi \right> $
\item
  $ \left | \cdots mn \cdots \right > \rightarrow \left | \cdots pq
\cdots \right > \Rightarrow \left < mn \right | \left | pq \right
  > $
\item
  $ \left | \cdots lmn \cdots \right > \rightarrow \left | \cdots pqr
\cdots \right > \Rightarrow 0 $
\end{enumerate}

Using these rules and a bit of algebra the Hamiltonian simplifies to
what's called the Fock operator with elements
\begin{equation}
  F_{\mu\nu} = \left< \mu \right| -\frac{1}{2}\nabla^2 \left| \mu \right>
  - \sum_{k}^{nuclei}Z_{k} \left< \mu \right| \nu \left> \right.
  + \sum_{\lambda \sigma} P_{\lambda \sigma}
  \left(
\left< \mu \lambda \right| \nu \sigma \left>\right.
- \frac{1}{2} \left< \mu \nu \right| \lambda \sigma \left>\right.
  \right)
\end{equation}

which can be substituted for H in equation \ref{eq:SchrodingerMatrix} to produce
We simplify this further by using the semi-empirical AM1, which uses predetermined
We can now apply the variational method to determine the coefficient of the wavefun
First, a trial density function is chosen, which is equivalent to a trial coefficie
We then solve the Roothan-Hall equation, save the lowest eigenvalue energy and use

We compare the energy differences between iterations until it's less than a chosen

\section{QM/MM}
    In this work, we will be focused on the behavior of a molecule after an electron ab
    In the previous sections we have discussed how quantum mechanics can be used for cl
    however, in many applications, the accuracy of QM is not needed and more computatio
    For these situations many computational chemist use classical electrical force fiel
    QM/MM was developed to manage computational costs by separating a calculation into
    This allows the user to have the accuracy where needed while not wasting resources
    For the vast majority of our calculations, we will have a QM solute and a few nearl
    The Hamiltonian for this system is
    \begin{equation}
     \mathbf{H}_{eff}=\mathbf{H}_{QM}+\mathbf{H}_{MM}+\mathbf{H}_{QM/MM}
    \end{equation}
    with
    \begin{align}\label{eq:qmmm}
      \mathbf{H}_{QM/MM}=-\sum_{e}\sum_mq_m\mathbf{h}_{electron}(\bar{r}_e,\bar{r}_m)\\
      +\sum_q\sum_mz_qq_m\bar{\mathbf{h}}_{core}(\bar{r}_q,\bar{r}_m)\\
      +\sum_m\sum_q\left(\frac{A_{qm}}{r_{qm}^{12}}-\frac{B_{qm}}{r_{qm}^6} \right)
    \end{align}
    where e, m, and q, are the electron, MM atom, and QM core indices respectivel
    q_m is the charge on the MM atom m, z_q is the charge on the QM atom q, $\bar

    Figure ? gives and example of a QM/MM systems.
    The atoms of the drawn out molecule will be described at the QM level of theory.
    The MM atoms in the volume immediately surrounding the molecular, label QMCut, wil
    To simulate a solute in solvent, we treat the provided box as a cell, that is repea
    Particle Mesh Ewald calculations are then used to calculate the long distance inter
    This is performed by treating the charge and potential in the long range, inter box
    Note that the QM region must be treated as single point charges for this calculatio
    The Mulliken charges of the current state are used for these calculations.
    Once the sums are complete, a fast Fourier transform is performed to obtain energy
    Charges from the MM region outside QMCut, will be used to provide a Particle Mesh

    Long range interaction, from those outside the cutoff, considered vital for the unc
    Trajectories use periodic boundary conditions to simulate an explicit solution, tre
    Particle Mesh Ewald calculations then determine the long-distance interactions of t
    Once the sums are complete, SQM performs a fast Fourier transformation to obtain th

    A general timestep would be as follow:

9

Calculate the MM ewald potentials using the classical charges from the MM atoms Co

Add the one electron terms for the interaction between QM atoms and the MM atoms w

Within the SCF routine, copy the Hamiltonian to the fock matrix, and add the two-el

Calculate the QM ewald potential using the iteration's Mulliken charges, then add t

The SCF procedure continues until convergence resulting in a density matrix that i

\section{Adiabatic Dynamics}
Excited-state calculations implement the Collective Electronic Oscillator (CEO) approac
The single-electron density matrix is defined by

    \begin{equation}
\rho_{g\alpha_{nm}}t = \left< \psi_\alpha t \right| c_m^\dagger c_n \left | \psi_g t \r
    \end{equation}

    where \(\psi_g\) and \(\psi_\alpha\) are the single-electron wave functions of the
    cm†(cn) is the creation(annihilation) operator summed over the atomic orbital \(m\)
    The basis set coefficients of these atomic orbits are calculated in the previous S
    The CIS approximation is applied, creating the normalization condition

    \begin{equation}
\sum_{n,m} (\rho_{g\alpha})^2_{n,m} = 1
    \end{equation}

    Recognizing that \(\rho_{g\alpha}\) represents the transition density from the grou

    \begin{equation}
\hat{\mathcal{L}}\bm{\rho}_{0\alpha} = \Omega \bm{\rho}_0\alpha,
    \end{equation}
    with \(\mathcal{L}\) being the two-particle Liouville operator and \(\Omega\) the e

    The action of the Liouville operator can be found analytically by
    \begin{equation}
\mathcal{L} \bm{\rho}_{o\alpha} = \left[\bm{F}^{\vec{R}} (\bm{\rho}_{00}),\bm{\rho
\left[\bm{V}^{\vec{R}} (\bm{\rho}_{0\alpha}), \bm{\rho}_{00} \right]
    \end{equation}

    where \(\bm{F}^{\vec{R}}\) is the Fock operator and \(\bm{V}^{\vec{R}}\) is teh col

The diagonalization of this Liouville equation of motions uses Davidson diagonaliza

The forces are then calculated analytically by the gradient of the ground state ene

```
\begin{equation}
\vec{\nabla} E_\alpha = \vec{\nabla} E_0 + \vec{\nabla}\Omega_\alpha
\end{equation}
```

With the gradient of the ground state being calculated by

```
\begin{equation}
\vec{\nabla}E_0 = \frac{1}{2} \text{Tr} \bm{t}^{\vec{R}} + \bm{F}^{\vec{R}}\bm{\rho
\end{equation}
and the gradient of the excited state being
\begin{equation}
\vec{\nabla}\Omega_\alpha = \text{Tr} \bm{F}^{\vec{R}} \left( \bm{\rho}_{\alpha\al
\end{equation}
where \(\rho_{ij}\) represents the density or transition density matrix for states
\(\bm{F}\) is the Fock matrix,
\(t\) is the the kinetic operator acting on one-electron, and \(\bm{V}\) is the co
```

\section{Non-Adiabatic Dynamics}

The MDQT approach utilized in this work as a modified version of the Tully Surface Hopp
Here the quantum wave function is approximated using a swarm of independent trajectorie
During time steps, these trajectories propagate along adiabatic surfaces;
However, between time steps, these trajectories are allowed to transition from one stat
That number oftrajectories in any given state corresponds to that state's quantum proba

We define the Hamiltonian

```
\begin{equation} \label{eq:tullyHamiltonian} \mathbf{H} = \mathbf{T}(\mathbf{R}) +
  \mathbf{H}_{el}(\mathbf{r},\mathbf{R})
\end{equation}
```

where \(\mathbf{T}(\mathbf{R}) \) is the nuclear kinetic energy operator and \(\textbf

We expand the the total wavefunction, \(\Psi\) into the adiabatic state wavefunctions \
```
\begin{equation}
```

11

```latex
  \Psi(\textbf{r}, \textbf{R}, t) = \sum_j c_j(t)\phi_j(\textbf{r}; \textbf{R}) = c_j \
\end{equation}
where \(\textbf{r}\) and \(\textbf{R}\) are the electronic and nuclear coordinates resp
```

The matrix elements of the electron Hamiltonian become

```latex
\begin{equation} \label{eq:tullyVelements}
  V_{jk}(\mathbf(R))=\left<\phi_j(\mathbf{r};\mathbf{R})\right|\mathbf{H}_{0}\left.(\ma
\end{equation}
```
and the time-dependent Shrodinger equation can then be written as

```latex
\begin{equation}
  i\hbar\dot{c}_j = c_k ( V_{jk} - i\hbar \left< \phi_j | \dot{\phi}_k \right> ).
\end{equation}
```
The term \(\left< \phi_j | \dot{\phi}_k \right>\) represents the coupling between the j

At each step we perform a montecarlo like decision

```latex
\begin{equation} \label{eq:tullyjump2}
\sum_{j=1}^{k-1}g_{ij} < \zeta  \le \sum_{j=1}^{k}g_{ij}
\end{equation}
```
hopping from state i to k when
```latex
\begin{equation} \label{eq:tullyjump1}
  \zeta < g_{ik}
\end{equation}
```
where \(\zeta\) is a uniformly distributed random number from 0 to 1, and

```latex
\begin{equation}
g_{ik} = \frac{b_{ki}(t=0)\Delta t}{a_{ii}(t=0)}
\end{equation}
```

with

```latex
\begin{equation} \label{eq:tullyb2a}
b_{kj} =
\frac{2}{\hbar}\Im\left(a_{kj}^*V_{kj}\right) - 2\Re\left(a_{kj}^*
 \dot{\mathbf{R}} \cdot \mathbf{d}_{kj}\right).
\end{equation}
```
a_{kj} are the off diagonals of the density matrix $a_{kj} = c_k^* c_j$ and

$\mathbf{d}_{kj}$ is the non-adiabatic coupling vector

\begin{equation} \label{eq:tullynacoupling}
\mathbf{d}_{kj}\mathbf(R) =
  \left<\phi_{k}(\mathbf{r};\mathbf{R})\right|\mathbf{\nabla}_{\mathbf{R}}\left.\phi_j(
\end{equation}
We use the Collect Oscillator Approach to calculate the non-adiabatic coupling terms \(
fly''. \textbf{cite:tommasini2001electronic,tretiak1996collective,tretiak2009representa

Inconsistencies arise from solely using the Tully surface hopping approach.
Trajectories transfer between the various adiabatic potential energy surfaces instanta
These coefficients are determined using the integral of the TDSE on multiple trajectori
Each trajectory if unmodified will keep in phase even after spatial separation.
Furthermore, if dealing with a system with a dense electronic state structure, its like
We apply a dechohence correction as well as a trivial crossing accounting system as pe

Implementation Details

Spectroscopic Analysis of PPV3-NO2

\chapter{Spectroscopic Analysis of PPV_3-NO_2}

Introduction

NEXMD is an efficient program for the simulation of photoinduced dynamics of extended
It includes solvent effects using implicit models. These implicit solvents provide insi
Many multichrormophoric molecular systems are soluble in polar solvents such as water,

Adequate sampling of the solvent and solute configuration space, including hundreds to
QM/MM methods exist to allow the computationally expensive QM calculations to be perfor
The SANDER program in the AMBER molecular dynamics package performs classical molecular
SANDER with QM/MM performs well with systems with tens of thousands of MM atoms and cur

In this work, we redirect AMBER's SANDER package from its usual semi-empirical QM packa
SANDER linked to the NEXMD library performs adiabatic dynamics at ground-state and CIS
We apply our method to an analysis of a three-ring para-phenylene vinylene oligomer (PP
We look at how explicit solvents affect PPV3-NO2's excited state structure as well as

Interface Design

Simulation Methods

Figure visually describes the layout of our simulations performed in vacuum, methanol, choroform, and carbontetrachloride. First, a molecular dynamics simulation of 320 ps was run in the ground state at 300K (NVT) using the General AMBER Force Field ground state Hamiltonian and periodic boundary conditions, as guided form previous convergence studies. 128 evenly spaced snapshots were collected from this simulation and used as intial conditions for another 128 individual 10ps-simulations equilibrated at 300K (NVT) using QM/MM ground state Hamiltonian. QM calculatations were performed using configuration interaction singles (CIS) with the AM1 hamiltonian which has previously been show to provide reasonable accuracy for computational cost. QM/MM excited state molecular dynamics simulations were run during 10 ps starting from the final configuration of each of the 128 ground state QM/MM trajectores by vertical excitation to the S1 state. A classical time step of 0.5 fs and a Langevin thermostat with friction constant of 2 ps-1 have been used either for ground state and excited state QMMM simulations. The CIS calculations include the first of excited states of the PPV3-NO2 molecule along with the stated number of solvent molecules closest to the central benzene ring. We treat all other solvent molecules using classical dynamics. We restrict the QM solvents from drifting away from the solute and the other MM solvents from drifting closer than these QM solvents.

As shown in Figure, the excited-state density resides towards the center of the molecule on the vinyl groups nearest to the phenyl group. Charge movements on solvents far from this concentration of density cause negligible energy differences. To maximize the utility of the QM/MM calculation, we only include the solute and the solvent molecules nearest to this central phenyl group in the QM calculations. To prevent these solvents from drifting during the trajectories, we implement a simple harmonic restraint using AMBER's NMR restraints. We select the N solvent molecules based on the proximity of the solvent atom closest to any atom located on the central benzene ring. We then restrain these solvents using the harmonic constraint on the distance from the center of geometry of the solvent to the center of geometry of the central phenyl group. We also restrain the solvent molecules not included in the QM calculation from getting closer to the central phenyl than the QM solvents, effectively making a spherical shield around the solute's central phenyl group. Since the distance between the

center of geometries and the closest atoms are not necessarily equal, solvent atoms could initially be pushed either inside or outside this shield during the transition from MM to QM. However, this push only occurs during the initial equilibration of the QM ground-state calculations excluded from any analysis. Once the QM calculations begin, these constraints persist throughout all further calculations. For our CCl4 simulations with the 5 nearest solvents included (CCl4-5QM), the restriction barrier had an average radius of 6.28 with the origin at the center of the central phenyl group.

Results

The structural differences between the excited-state and ground-state of PPV3-molecules are presented clearly by distortions in the C=C and C-C bonds found in the vinylene segment. These distortions can be measure by bond length alternation (BLA)

$$\frac{d_i + d_e}{2} - d_e, \tag{1}$$

where d_i and d_e are the interior and exterior bonds, and d_c is the central bond. This value represents the differences between the double and single bonds of the vinylene sections. The BLA is a descriptor for π bond distributions. In this system, we analyze the BLAs of two separate bond sets, the bonds d1-3 (near-set) and d4-6 (far-set) seen in Scheme 2.

Figure show the bond length alternation of PPV3-NO2 in various solvents during the S1 trajectories where the dashed lines represent equilibrated ground state values which are near 0.110 Å for sets d1-3 and d4-6 regardless of solvent enviornment. Within the first couple hundred femtoseconds after the excitation to S1, the central bonds expand, while the interior and exterior bonds contract. For all solvent environments, this bond restructuring is amplified by close proximity to the amino group, where we see an average drop of 0.07 Å in sets d1-3 compared to a 0.04 Å drop in sets d4-6. The strength of this amplification is dependent on the solvent environment where the BLA difference between the far and near sets PP3-NO2 in methanol, 0.034 Å, surpases that found in carbon tetrachloride, 0.022 Å.

Table 2 presents further details of the S1 BLA simulation. In all cases, the exterior bond (d1 and d4) becomes slightly longer than the interior bond (d3 and d6). The BLAs from the near and far sets therefore split. In the near set, the S0 and S1 BLA converge to 0.1091 Å and 0.00453 Å, respectively. In the far set, these numbers are 0.1103 Å and 0.0697 Å, respectively. The smaller bond length spread in the near set, along with the lower BLA, suggests more delocalization on those bonds than in the far set.

15

The number of solvents included in the QM calculations had little effect on the convergence of the distances or BLA. PPV3-NO2 had similar ground state BLAs of around 0.11 Å for both near and far sets matching results on similar systems regardless of the solvent. The information presented is averaged over time after relaxation across all trajectories. The S1 BLAs varied between the solvents and with the distance away from the NO2 group. Among the selected solvents, CH3OH has the smallest near set S1 BLA and largest far set S1 BLA. CCl4 has the largest near set S1 BLA, and also the smallest far set S1 BLA and has close to vacuum-like behavior. The CH3OH solvent seems to enlarge the BLA changes from the ground to excited states. The significant effects of S0-S1 transitions on the Cartesian measurement of BLA encourages the analysis of these bonds' quantum mechanical behavior. Because the double bonds elongated and the single-bonds contracted, we expect the single-bonds to gain a partial double-bond character and vice versa. Simple bond ordering does not consider these subtleties of a quantum electronic wave-function. Fortunately, the quantum mechanical descriptor, Wiberg bond index, provides a reasonable analogy of the classical Lewis structure a chemist would expect. Wiberg bond indexes are calculated from the density matrix by

$$W_{AB} = \sum_{\mu \in A} \sum_{\nu \in B} |D_{\mu\nu}|^2 \tag{2}$$

where A and B are indexes of the two atoms, μ and ν are the atomic orbitals, and D is the density matrix. The method sums the electron density shared by both atoms. If an electron if fully localized on a single atom, the sum of the elements equals zero providing a value that matches our intuition of a bond.

As the bond order increases, we expect the bond to become more rigid and the bond length to shrink. Figure ? displays the bond order of bonds d1-6 for PPV3-NO2 in CCl4 with 5 QM solvent molecules. At time t=0, the system instantaneously transitions to the first excited state, S1. The Wiberg bond index then uses the density matrix for S1, leading to a sudden shift in its value. At S1, the bond orders of d2 and d5 instantaneously drop, and expansion of their bond lengths soon follows. The larger shifts in the near set correspond to the information found in the BLA analysis. The interior bonds, d1 and d4, have lower bond indexes than their exterior counterparts, d3 and d6. We use the torsion angle around the vinylene segments as the slow nuclear coordinates of PPV3-NO2-molecules following precendent. In PPV3-NO2 systems, the excitation to S1 leads to relaxation towards a nearly planar structure Torsion angle around 1,3 and 4,6 are averaged over 128 trajectories

to produce the near and far torsion angle data respectively.

For our CCl4-5QM example, the dihedral angle around the near set d1 to d2 equilibrates around 23° and 12° in the S0 and S1 states, respectively. For the near set, d4 to d6, these values are 23° and 15°. Once again, only a noticeable difference in S1. The time constants for the S1 dihedral relaxations are around 0.8 ps. Relaxation of the dihedral angles occurs by four ps.

Table 5 shows a summary of the torsion angles analysis of all tested solvents after five ps of relaxation after the jump to the first excited state. The trajectories include 20 solvent molecules within the QM calculations. A noticeable shift towards a planar geometry occurs in all solvents. This shift is greatest near the nitro group.

Energy Relaxation

The absorption and the fluorescence properties are judged primarily through the difference between the ground state (S0) and the first excited state (S1) energies. The system starts at the S0, where it remains near the bottom of the energy well. Figure 6 shows the energies for states S0 and S1 averaged over 128 trajectories for PPV3-NO2 in CCL4 with five solvent molecules included in the QM calculations. During the first six ps, the system runs on the ground-state S0, and the S0 energies stay near the minimum with small oscillations caused by temperature. At the time 0 ps, the system instantaneously hops to the S1 potential energy surface. The average energy difference at t=0 between S0 and S1 is 2.93 eV, and it corresponds reasonably well with the peak of the absorption spectrum. When the system relaxes on the new surface, the S1 and S0 energies decrease and increase respectively, until the difference between the two is 2.50 eV agreeing with the peak found in the fluorescence spectra. Table 7 presents the fitted decay of S1 energies using

$$E = E_d \mathrm{e}^{-t/\tau} + c \tag{3}$$

where E_d is the relaxation energy drop, τ the time constant, and c the steady state energy at S1.

Spectra

Energies, coordinates, and dipole information are acquired every ten steps. Equilibration times from either MM to QM state or from the S0 to S1 state range from 2-4 ps. We exclude the first four ps of each trajectory in the

17

calculation of the spectra in data analysis for the absorption and emission analysis.

Previous studies have analyzed solvatochromic shifts in conjugated substituted PPV3-NO2 molecules with the NEXMD program in implicit solvents. Results with NEXMD by TD-AM1 were redshifted from the experimental results, while single-point calculations using TD-CAM-B3LYP provided by G09 in the same implicit solvent were blue shifted. Other NEXMD computations have shown comparable redshifts in spectra of similar molecules in implicit solvents compared to experiment. We performed similar calculations in this paper; however, in explicit solvent. We compare the results to those presented in implicit solvent.

We collect the vertical excitation dipoles and oscillator strengths between the ground state S0 and S1 every five fs during the steady-state of each trajectory to produce the absorption/emission spectra of PPV3-NO2. We sum over excitation states averaged over the geometries and broaden the spectra using a Gaussian bin function with FWHM=0.16 eV corresponding to a 100 fs FWHM laser excitation. We normalized it such that the maximum absorption is 1.

Figure ? presents the absorption spectra for PPV3-NO2 in select solvents and vacuum. The shown absorption has contributions from the nine lowest energy excited states, though the S1 state is the primary contributor to the spectra. We found the number of solvent molecules included in the QM region caused only minor deviations in the spectra, with the largest variance (0.02~eV) occurring between the 20QM and MM CCL4 systems, as such, in figure 12, we only present results from trajectories with 20 QM solvents. All solvent results are redshifted from those in vacuum matching findings in previous works. The absorbance within methanol and chloroform were very similar, with a peak shift from vacuum of -0.04 eV. Within carbon tetrachloride, this shift increases slightly more to-0.06 eV.

Aligning with previously reported results, the fluorescence calculations found in figure 13 show an overall more intense redshift from vacuum, along with a more significant dispersion among the solvents. The smallest shift, at -0.06 eV, occurs in carbon tetrachloride, while the largest, at -0.12 eV, occurs in methanol. Previous works have demonstrated that the energy levels of PPV3-NO2 are further stabilized by more polar solvents, a feature clearly seen by our results.

Conclusion

The Non-adiabatic Excited State Molecular Dynamics package (NEXMD) that SANDER is linked to for the excited state calculations done in this paper is designed to perform molecular dynamics simulations outside the Born-Oppenheimer approximations using the FSSH in implicit solvents. The program has been tested well and is helpful in gaining insights into the dynamics of molecules prone to photo-excitations. However, simulations in explicit solvents have been shown to produce qualitatively different results than in implicit solvent mediums. By linking AMBER's SANDER to NEXMD, we produced a quick and efficient tool to simulate explicit solvent behavior on adiabatic excited state dynamics.

Non-Adiabatic Decay of PPV3-NO2

Introduction

During ultra-fast photovolatic processes, the Born-Openheimer appoximation breaks, and accounting for non-adiabatic behavior become necessary. These situations occur frequently within processes of interest to photochemistry and photophysics. For example, the excitation to a non-equlibrium state followed by a relaxation through internal conversion is a process common to processes such as photosynthesis, solar-cell photo-absoprtion, optical detectors, and the excitation of the visual nerve. Multiple methods to have been proposed and used to simulate these non-adiabatic processes. These methods include treating the nuclear coordinates quantum mechanically or similclassically, or by using a hybrid quantum mechanical, classical treatment to account for the non-adiabaticity. One of the more popular version of the latter, and the one which we use in this work, is Molecular Dynamics with Quantum Transitions (MDQT), were the system propogates classically along adiabatic potential energy surfaces, but a quantum evalutation is made at each time step to determine whether to transition to another state.
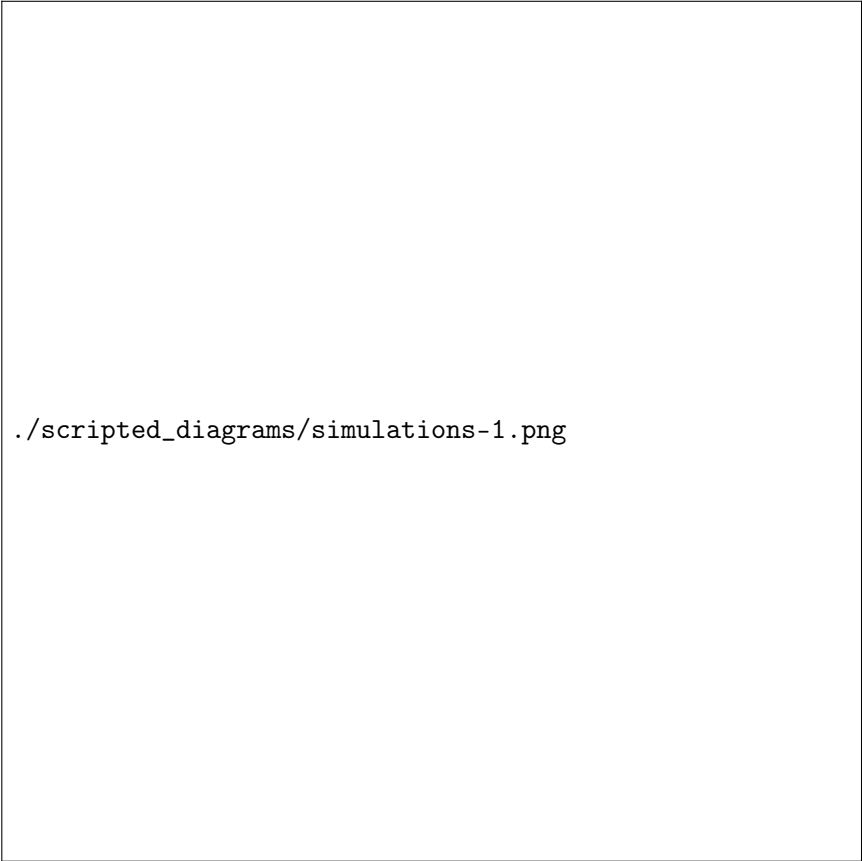
For many areas in which nonadiabatic dynamics simulations would be of interest, solvents play a crucial role. In situations where ultrafast electronic relaxations occur, the electronic decay is often faster than the time for the solvent to equilibrate. As such, Implicit solvents, which adjusts instantaneously to any changes, become imprecise approximation However performing non-adiabatic dynamics on such large systems is far too computationally expensive. To ease the computational cost we can employ QM/MM methodologies to perform the non-adiabatic calculation only on the areas of

interest. Similar methods have been employed in the study of retinal photochemistry and organic semiconductors. In this work we implement a new method of performing non-adiabatic QM/MM using the SANDER package AMBERTOOLS combined with the high performance Non-Adiabatic simulator NEXMD. We further analyze the effects of including near solvent molecules within the QM region.

NEXMD, currently being developed by the Tretiak lab in los Alamos, has a proven track record of performance on the stimulation of ultra-fast non-adiabatic behaviors. It's ability to solve state coupling equations on-the-fly has found great utility for systems with hundreds of atoms. Numerous studies have implemented the method for research into topics including the study of chlorophyll organic conjugated molecules, and pi conjugated macro-cycles. Such studies with NEXMD have been limited to implicit solvents. No method to provide NEXMD with QM/MM capabilities have yet to be implemented.

Amber is primarily known as a classical force-field molecular dynamics package. It's a massive project maintained by people across the globe that's been designed to work with very large systems ranging in the tens of thousands of atoms. Amber is capable of a huge range of simulations from replica exchange to QM/MM umbrella sampling using nudge elastic bands. Most importantly for this research, it has a proven track record of doing QM/MM solvent-solute simulations using periodic boundary conditions.

Methods

We equilibrated the system to a temperature set to 300K. To collect a broad enough sampling, we sampled from a 1024 ps, with a 0.5 fs timestep fully classical trajectories using the AMBER force field. We performed a separate trajectory for each situation combination of solute / with solvent including whether the solvent was included in the QM calculations. We had a total of 6 separate 1024 ps classical trajectories, PPV3 in Vacuum, CH_{3OH}, and 5QM CH_{3OH} and PPV$_3$-NO$_2$ in Vacuum, CH_{3OH}, and 5QM CH_{3OH}. 1024 snapshots where taken at 1ps, 2ps .. 1024ps. We used the final frame of those tranjectories as the initial conditions for an additional 4ps using the AM1 semiempical Hamiltonian Born-Oppenheimer on the molecules to be included in future QM calculations to allow the system to relax. The 4 ps timescale was determined using the information form the previous paper. The simulations were described the Langevin equations at a temperature set to 300 K with the Langevin friction parameter set to 2 ps^{-1}. The final

frames of these QM trajectories were then used as the initial conditions for the following pulse pump calculations. Pump-Probe Spectroscopy is an experimental technique commonly performed in the study of ultrafast electonic statte dynamics. In the case of conjugated polymers in can be used to study the localized excictronic transitions that are accessible through an excitation from the S1 state but not the ground state S0. To simulate this behavior, we take the final snapshot of the QM ground state calculations and perform a single point calculation at the S1 state to find the next state with the highest oscillator strength.
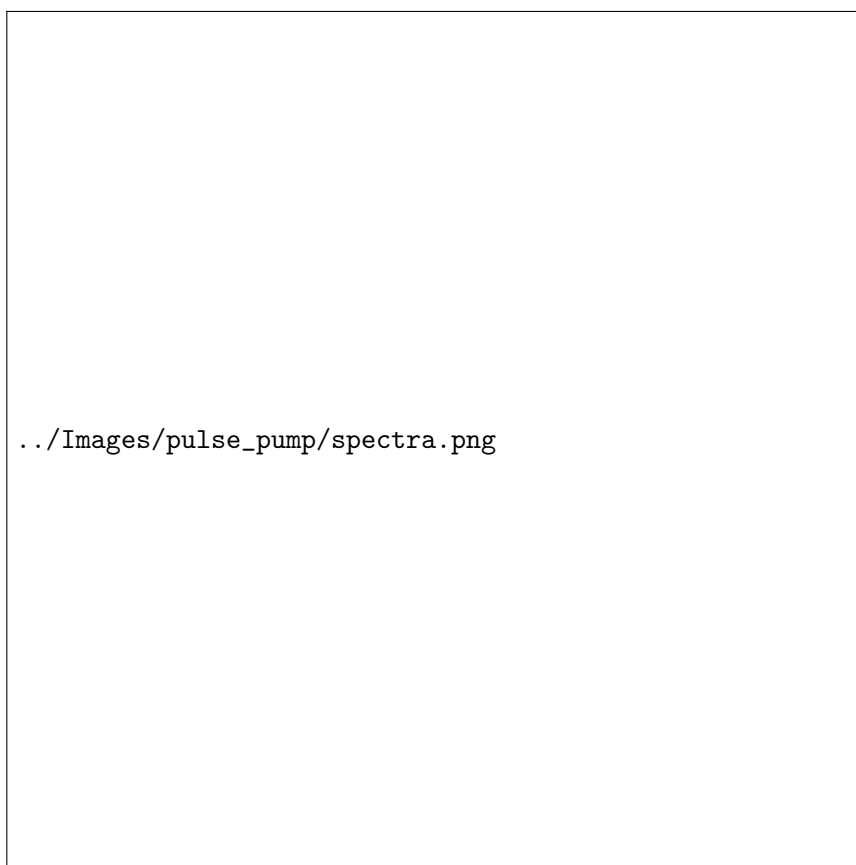
../Images/pulse_pump/spectra.png

Figure 1: The calculated S_1 state absoprtion spectrum from the ground state geometries.
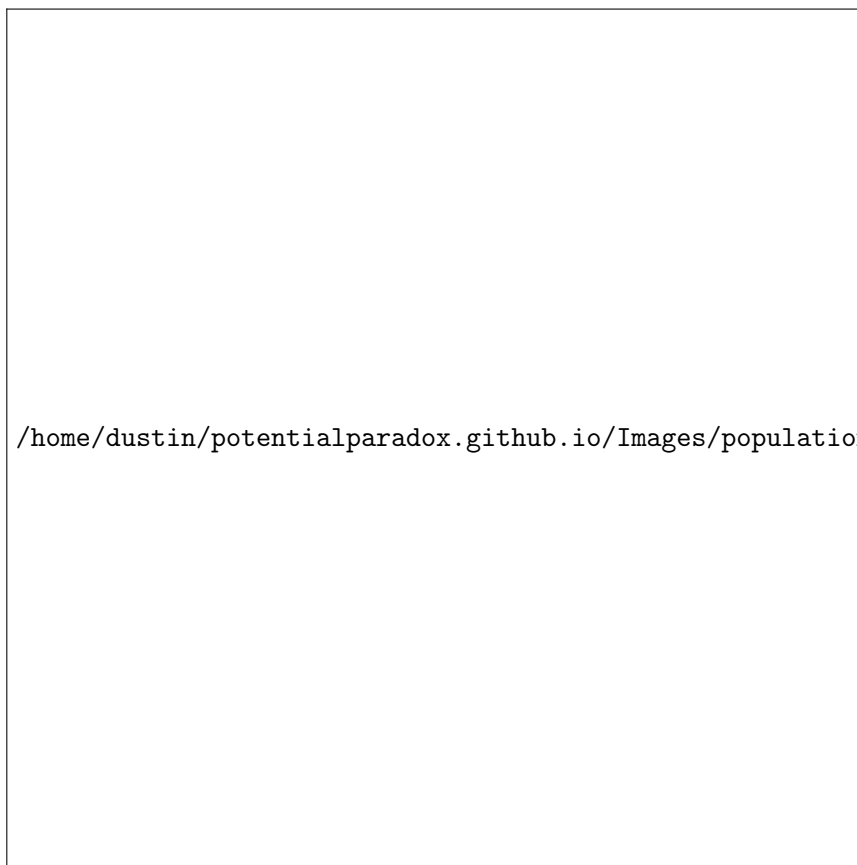
Results

State Popultations

Figure 2: Comparison of the population decays or rises of states S_1, S_2, and the initial state S_m between simulations with varying number of solvents included in the QM region.

Figure **??** shows the population of each state calculated as the number of trajectories at the state's potential energy surface over the total number of trajectories. S_m represents the initial state calculated using the pulse pump calculations previously done. States S_7 and S_9 are included as the only other "slow" states, or states that reached a population of more than 0.05. The other states were excluded from the graph. These charts show that the addition of the NO_2 oligimors dramatically speed up the state relaxation.

Table 1: Fitting Parameters for the model of the rise of the S_1 population.

Solvent	τ (fs)	A
Vacuum	89.9	1.61
CH$_3$OH	97.8	1.53
CH$_3$OH with 5QM	119.5	1.53
CH$_3$OH with 10QM	122.0	1.54

S_m ranged from S_9 to S_{15} for PPV$_3$ and S_{11} to S_{21} for PPV$_3$-NO$_2$. Figure **??**, shows the rise of the S_1 populations over the first 500 fs after excitation. We model these rises by fitting the curves to the function

$$f(t) = \frac{Ae^{t/\tau}}{A + e^{t/\tau}} - \frac{A}{1 + A} \tag{4}$$

where t is time, τ is the relaxation, and A is a constant that normalizes such that the populations remain between 0 and 1. The results are displayed in 1. We clearly see that adding a test for trivial-nonavoided crossing slows the rate of relaxation from a time constant of 258˜fs. This is to be expected since we are now preventing transitions (mostly downward) that should not occur. The methanol have mixed results with regards to PPV3 and seem to slightly slow the relaxation of PPV3-NO$_2$. Experiments using ultrafast spectroscopy have shown that for PPV thin films the time constant for relaxations should be around 200 fs. However, that was on thin films and for PPV$_3$, the energy gap !! Average S_1 -> S_m energy gap) than in the thin film (0.8eV). Previous research using the NAESMD framework have shown a time constant of 394 fs, but this was without the test for trivial non-avoided crossings.

Potential Energies

Bond Length Adjustment

Dihedral Angles

The torsion angle around the vinylene segments have been shown to be highly coupled to the excited state. [?, ?]

Wiberg Bond Analysis

Conclusion

Figure 3: Potential energy difference from the intial ground state during dynamics averaged over trajectories.

../Images/bla/solvent_comparison.png
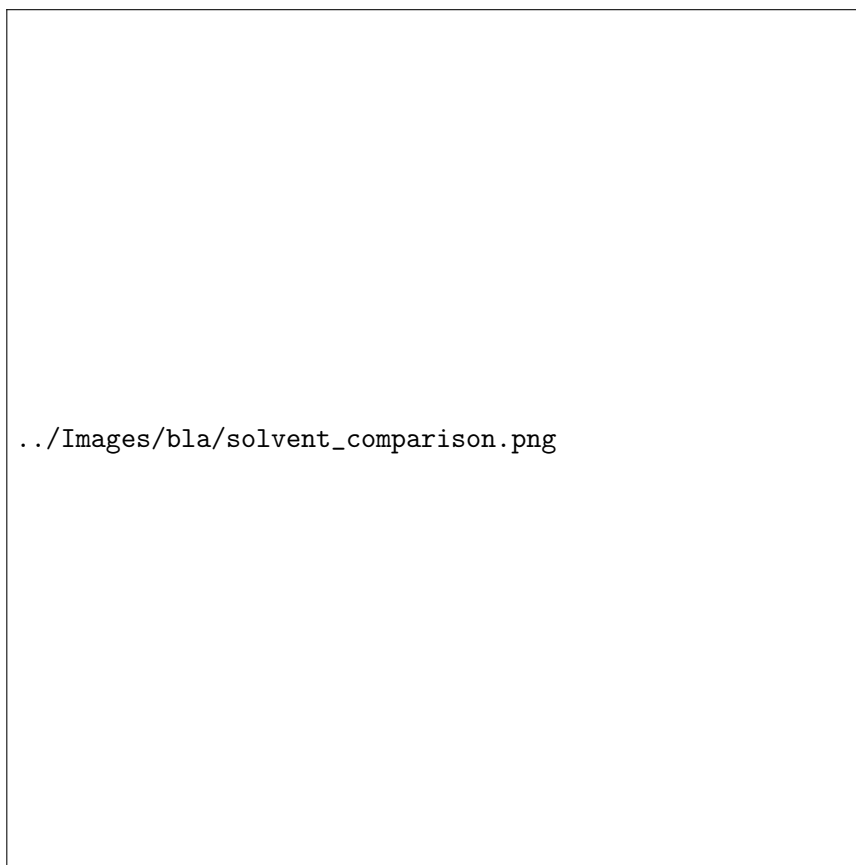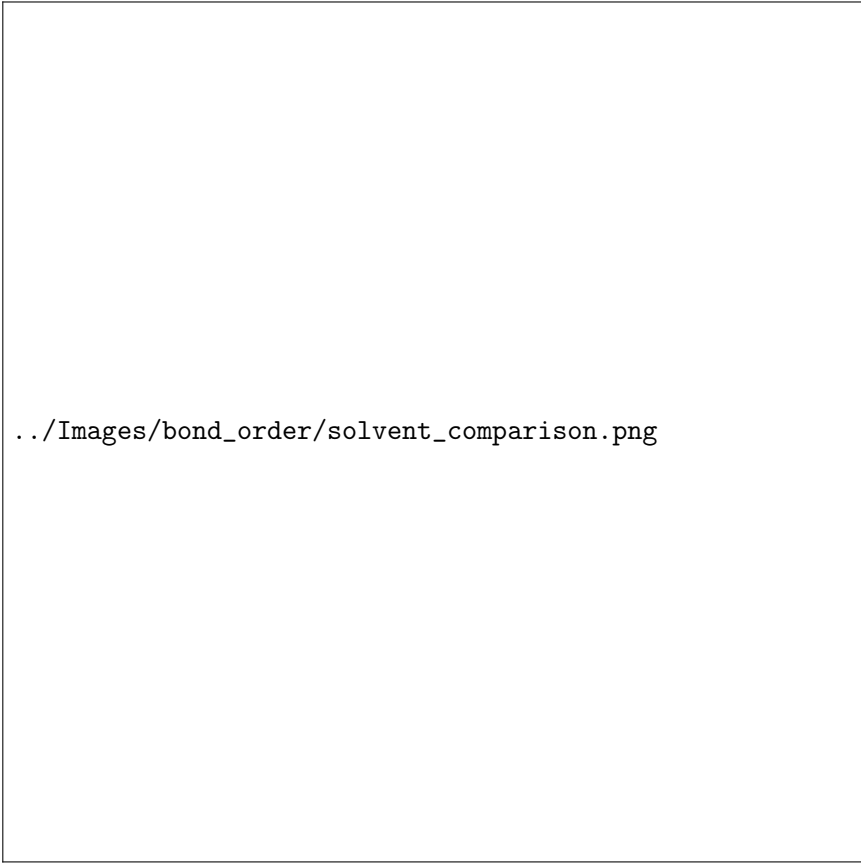
Figure 4: Bond Length Adjustments for various states for PPV_3 and PPV_3-NO_2 in vacuum.

Figure 5: Dihedral angles for various states for PPV$_3$ and PPV$_3$-NO$_2$ in vacuum.

../Images/bond_order/solvent_comparison.png

Figure 6: The Wiberg Bond Orders averaged over the ensemble of trajectories for select bonds for $PPV_3\backslash_{NO2}$ with various number of solvents included in the QM region.